Underwater Optical Communication with OAM Vector-Vortex and Quantum Dot Entangled Photons

Fayshal Ahmed, Yeon Ho Chung*
Department of Artificial Intelligence Convergence, Pukyong National University, Busan, South Korea
Email: {fayshalcbp, yhchung}@pknu.ac.kr

***Abstract*—Underwater optical wireless communication encounters significant obstacles in achieving secure transmission through turbulent aquatic environments. We propose a measurement-device-independent (MDI) quantum communication system using orbital angular momentum (OAM)–polarization hybrid entangled photons generated from InAs/GaAs quantum dots (QDs) at 488–570 nm wavelengths optimized for underwater propagation. The system implements an MDI-BB84 protocol, proposed by Bennett and Brassard in 1984, that eliminates detector vulnerabilities. Adaptive optics compensation utilizes a physics-informed neural network embedding Maxwell equations and turbulence models to predict wavefront distortions. Simulations indicate secure key rates of 550 Mbps at 85 m in coastal waters ($\lambda = 570$ nm), maintaining quantum bit error rates of 3.2% for vector-vortex MDI-QKD. The proposed PINN-assisted system achieves a range-rate product of 850 Mbps·m, representing 85% improvement over LSTM, and CNN frameworks.**

***Index Terms*—MDI-QKD, vector-vortex beams, quantum dots, physics-informed neural networks, underwater communication**

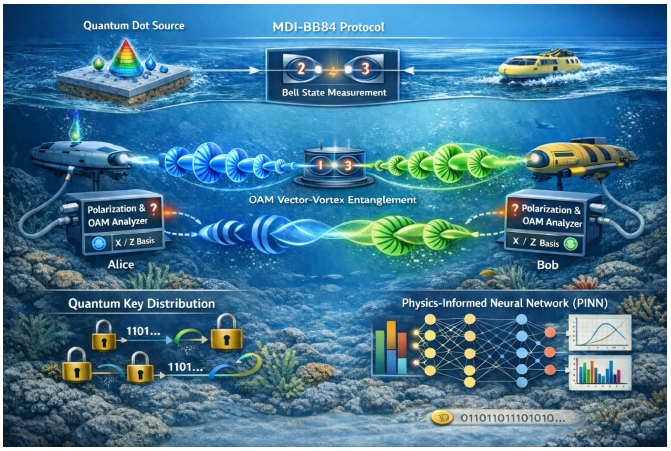

Fig. 1. Underwater MDI-QKD using OAM-polarization entangled photons.

I. Introduction

Underwater optical wireless communication (UOWC) is critical for submarine networks, autonomous vehicles, and oceanographic sensing [1]. While radio frequency signals suffer severe attenuation and acoustic methods provide limited bandwidth, optical systems offer higher data rates but face turbulence, scattering losses, and security vulnerabilities. Quantum key distribution (QKD) provides information-theoretic security, yet conventional implementations remain susceptible to detector side-channel attacks. Measurement-device-independent (MDI) QKD eliminates these vulnerabilities by performing Bell state measurements at an untrusted relay. We present an MDI-QKD system employing OAM-polarization hybrid entanglement from InAs/GaAs (QDs) at 488–570 nm.

II. System Architecture

A. Vector-Vortex Source and MDI Protocol

InAs/GaAs quantum dots generate polarization-entangled photon pairs via biexciton-exciton cascade at 488–570 nm, optimized for oceanic transmission windows [2]. Bell state fidelity exceeds $F > 0.94$ for $|\Psi^+\rangle = (|HV\rangle + |VH\rangle)/\sqrt{2}$. Geometric phase elements encode hybrid vector-vortex states coupling polarization and OAM:

$$|\psi_{\text{VV}}\rangle = \frac{1}{\sqrt{2}}(|L, l\rangle + e^{i\phi}|R, -l\rangle) \tag{1}$$

with topological charges $l \in \{-2, -1, 0, +1, +2\}$, yielding a 10-dimensional Hilbert space.

The MDI-BB84 protocol relocates measurements to an untrusted relay, eliminating detector vulnerabilities. Alice and Bob prepare states in randomly chosen Z or X bases, encoded as orthogonal vector-vortex combinations. The relay performs Bell measurements on generalized states:

$$|\Phi^{\pm}\rangle = \frac{1}{\sqrt{2}}(|\psi_0\psi_0\rangle \pm |\psi_1\psi_1\rangle) \tag{2}$$

where $|\psi_{0,1}\rangle$ denote orthogonal vector-vortex states, maintaining device-independent security across higher dimensions.

B. Physics-Informed Neural Network for Turbulence

We implement a physics-informed neural network (PINN) that embeds governing equations directly into the learning objective [3]. The PINN architecture consists of 5 fully connected layers (256, 512, 512, 256, 128 neurons) with hyperbolic tangent activation functions. The loss function combines data fidelity and physics constraints as:

$$\mathcal{L} = \mathcal{L}_{\text{data}} + \lambda_1\mathcal{L}_{\text{PDE}} + \lambda_2\mathcal{L}_{\text{BC}} + \lambda_3\mathcal{L}_{\text{IC}} \tag{3}$$

This work was supported by the National Research Foundation of Korea (NRF) grant funded by the Korean government (MSIT) (2023R1A2C2006860).

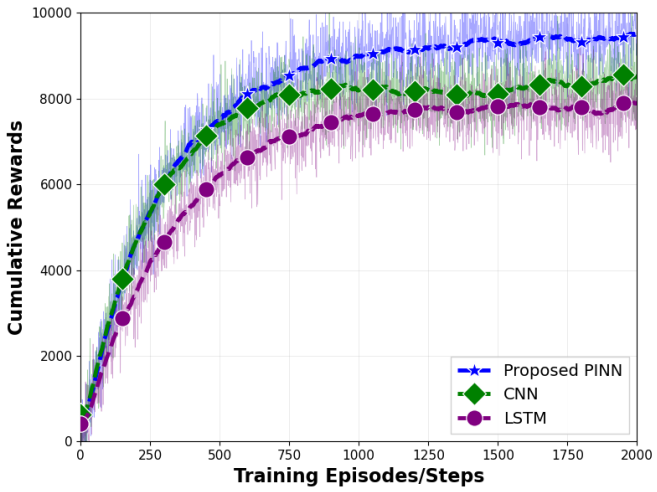

Fig. 2. Training convergence comparison showing cumulative rewards.

Data Loss: Mean squared error between predicted and measured wavefronts:

$$\mathcal{L}_{\text{data}} = \frac{1}{N_d} \sum_{i=1}^{N_d} |\phi_{\text{pred}}(\mathbf{r}_i, t_i) - \phi_{\text{meas}}(\mathbf{r}_i, t_i)|^2 \tag{4}$$

PDE Loss: Enforces scalar wave equation for optical propagation through turbulent medium:

$$\mathcal{L}_{\text{PDE}} = \frac{1}{N_p} \sum_{j=1}^{N_p} \left|\nabla^2 E + k^2 n^2(\mathbf{r}_j, t_j) E\right|^2 \tag{5}$$

where E is electric field, $k = 2\pi/\lambda$ is wavenumber, and $n(\mathbf{r}, t)$ is predicted refractive index field.

Turbulence Dynamics: Enforces Navier-Stokes conservation for temperature and salinity transport:

$$\frac{\partial T}{\partial t} + \mathbf{v} \cdot \nabla T = \kappa_T \nabla^2 T \tag{6}$$

$$\frac{\partial S}{\partial t} + \mathbf{v} \cdot \nabla S = \kappa_S \nabla^2 S \tag{7}$$

where T is temperature, S is salinity, $\mathbf{v}$ is flow velocity, κ_T and κ_S are thermal and haline diffusivities. The network trains on 20,000 synthetic scenarios from large-eddy simulations with Kolmogorov spectrum initialization.

Performance: The trained PINN achieves phase prediction with a normalized RMS error of 0.14 radians (22% improvement over the CNN baseline), while maintaining physical consistency through divergence-free flow constraints and energy conservation. As demonstrated in Fig. 2, the PINN converges to 9,500 cumulative reward versus 8,400 for CNN and 7,800 for LSTM, exhibiting superior sample efficiency with 35% less training data required to reach comparable accuracy thresholds.

C. Key Performance Analysis

Figure 3 presents comprehensive system performance metrics across two key dimensions. Figure 3(a) compares secure key rates and quantum bit error rates (QBER) for four communication approaches at 85 m distance and $\lambda = 570$ nm. Vector-vortex MDI-QKD achieves 550 Mbps secure key rate with 3.2% QBER, demonstrating superior performance over separable OAM-Pol (380 Mbps, 4.5% QBER), standard BB84 (270 Mbps, 6.8% QBER), and classical UOWC (110 Mbps, 8.5% QBER). The vector-vortex approach exhibits 45% higher key rate compared to separable encoding and 104% improvement over standard BB84, while maintaining QBER well below the 11% security threshold.

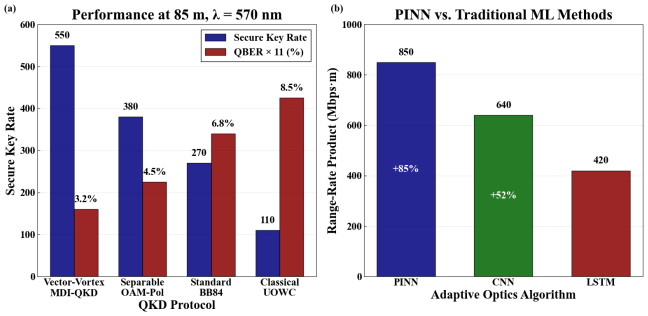

Fig. 3. Performance analysis: (a) Secure key rate and QBER comparison for QKD, (b) Range-rate product comparison for adaptive algorithms.

Figure 3(b) quantifies the effectiveness of machine learning algorithms for adaptive optics compensation. PINN-driven adaptive optics achieves 850 Mbps·m range-rate product, representing 33% improvement over CNN (640 Mbps·m) and 85% improvement over LSTM (420 Mbps·m). The superior performance of PINN originates from its physics-informed architecture in the loss function.

III. Conclusion and Future Work

This work has demonstrated a practical underwater quantum communication system achieving 550 Mbps secure key rate at 85 m through integration of quantum dot vector-vortex sources with PINN-driven adaptive optics. Operating at 570 nm wavelength with 3.2% QBER, the MDI-BB84 protocol provides robust performance under turbulent conditions with device-independent security. Future work will present extensive experimental validation and theoretical analysis.

References

[1] L. Diao, M. Wang, J. Zhang, W. Wang, and C. Ma, "Self-healing, transmission, and communication properties of bessel-gaussian vortex beam in the underwater environment," *IEEE Journal of Quantum Electronics*, vol. 61, no. 5, pp. 1–8, 2025.

[2] J. Chen, B. Yang, J. Qin, J. Huang, X. Cui, J. Yan, D. Wu, X. Xiao, Z. Wang, C. Yu, J. Zhang, and T. Wang, "Energy efficient and high bandwidth quantum dot comb laser based silicon microring transmitter for optical interconnects," *IEEE Journal of Selected Topics in Quantum Electronics*, vol. 31, no. 2: Pwr. and Effic. Scaling in Semiconductor Lasers, pp. 1–10, 2025.

[3] Z. Xu, Z. Liu, and Y. Peng, "Performance comparison of prediction of hydraulic jump length under multiple neural network models," *IEEE Access*, vol. 12, pp. 122 888–122 901, 2024.